Measurement of two-electron contributions to the ground-state energy of heliumlike ions

R. E. Marrs and S. R. Elliott*
Lawrence Livermore National Laboratory, Livermore, California 94550

Th. Stöhlker
Gesellschaft für Schwerionenforschung, 64220 Darmstadt, Germany
(Received 21 February 1995)

We report direct measurements of two-electron contributions to the ground-state energy of high-Z heliumlike ions. The difference in radiative-recombination x-ray energy (i.e., ionization potential of the recombined ion) was measured for bare and hydrogenlike target ions trapped in an electron-beam ion trap for six elements ranging from $Z=32$ to $Z=83$. The achieved uncertainties (as small as 1.6 eV) test the second-order many-body contributions to the energy and approach the size of the two-electron (screened) Lamb shift. We also report a measurement of the ground-state ionization potential of heliumlike bismuth relative to heliumlike xenon. All results are in agreement with available theories.

PACS number(s): 32.10.−f, 34.80.Kw, 32.30.Rj

I. INTRODUCTION

Spectroscopic studies of the energy levels of few-electron high-Z ions can be used to understand the effects of quantum electrodynamics (QED) and multielectron contributions in strong Coulomb fields. These effects appear as a difference between the physical energy and the Dirac-Coulomb energy of an atomic state. For one-electron systems this difference is the Lamb shift and is commonly expressed as

$$L=\frac{\alpha}{\pi}\frac{(Z\alpha)^4}{n^3}F(Z\alpha)m_0c^2, \tag{1}$$

where α is the fine-structure constant, n is the principal quantum number, m_0c^2 is the electron rest mass (in energy units), and $F(Z\alpha)$ is a slowly varying function of Z that contains all the necessary (mostly QED) corrections [1]. At high Z, $F(Z\alpha)$ is dominated by higher-order terms in $(Z\alpha)$ that are not important at low Z.

Experimental studies of hydrogenlike low-Z ions provide a measurement of the lower-order self-energy corrections with extraordinary precision. For high-Z ions, the higher-order self-energy corrections and the vacuum polarization are the most important QED contributions that cannot be tested with low-Z ions. In addition, a correction for finite nuclear size becomes important at very high Z. Precision x-ray spectroscopy measurements are required to test these high-Z corrections.

The one-electron (hydrogenlike) ions are the easiest to treat theoretically and calculations of their energy levels are thought to be highly accurate even for very high Z [1]. The accuracy of the measured ground-state Lamb shift in hydrogenlike high-Z ions has recently been improved by an order of magnitude with experiments performed at the ESR heavy ion storage ring in Darmstadt. In this case, Lyman-α transitions were measured with uncertainties of 8 eV for gold [2,3] and 16 eV for uranium [4,3], as compared with a total one-electron Lamb shift of 458 eV [5] for the hydrogenlike uranium ground state.

The heliumlike ions are the simplest multielectron system. However, in contrast to the hydrogenlike ions, there is no exact solution for the structure of high-Z heliumlike ions. Although substantial progress in the theory of two-electron ions has been achieved, there are still important QED contributions that have not yet been calculated [6–9]. The two-electron contribution to the energy of a heliumlike ion includes, in addition to the dominant Coulomb term, effects from electron correlation, the Breit interaction, screening of the Lamb shift, and higher-order radiative corrections.

Although precision spectroscopy measurements of $K\alpha$ transitions in heliumlike ions are available for $Z\leqslant 36$, theory has not been well tested at higher Z. At high Z, the individual $K\alpha$ transitions are incompletely resolved in present experiments [10–13], which precludes a measurement at the level of precision available for hydrogenlike ions. This relatively low precision of the available high-Z heliumlike measurements does not allow a sensitive test of the theoretical predictions for the ground-state energies.

Here we report the results of an experimental approach that exploits radiative recombination (RR) transitions into the vacant $1s$ orbitals of bare and hydrogenlike ions for a direct measurement of the two-electron part of the ground-state energy in heliumlike ions. We measure the difference in the energy of RR x rays emitted in electron capture by stationary bare and hydrogenlike target ions. This difference is equal to the difference in the ionization potential between the hydrogenlike and heliumlike ion, which is exactly the two-electron contribution to the ground-state energy of the heliumlike ion. It should be noted that the one-electron contributions to the energy, such as the finite-nuclear-size correction and the one-electron self-energy, cancel out in this type of experiment, which makes such measurements unique.

We have obtained data for Ge ($Z=32$), Xe ($Z=54$), Dy ($Z=66$), W ($Z=74$), Os ($Z=76$), and Bi ($Z=83$). We also report a measurement of the difference in the heliumlike ionization potentials of bismuth and xenon. This comparison

*Present address: University of Washington, Seattle, WA 98195.

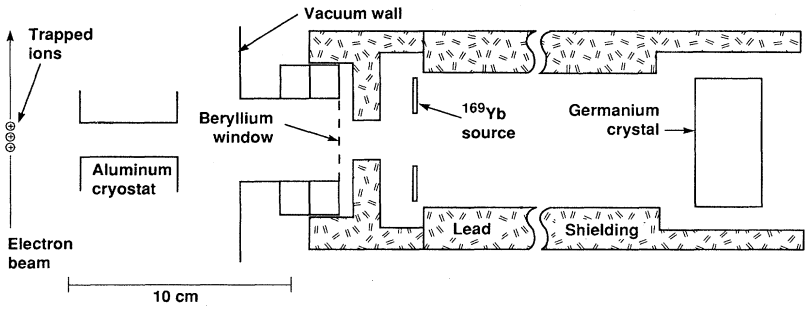

FIG. 1. Experimental arrangement used for the ionization potential measurements. The ^{169}Yb source consists of several removable pieces attached to an annular holder. The detector was located 46 cm from the trapped ions.

tests theory in a different way because it is most sensitive to corrections that have the strongest Z dependence and the one-electron contributions do not cancel out. In contrast to accelerator measurements, where Doppler shift corrections make a large contribution to the experimental uncertainty, the accuracy of our results is essentially limited only by counting statistics.

II. EXPERIMENTAL METHOD

Our measurements were performed with the super electron-beam ion trap (Super EBIT) at the Lawrence Livermore National Laboratory. This device can produce bare and hydrogenlike target ions of any element trapped in an electron beam of arbitrary energy up to 200 keV [14]. The x-ray spectrum from the trapped ions contains a series of RR lines at energies above the electron-beam energy, corresponding to electron capture into the open shells of the target ions. Normally, several charge states of a selected element are present simultaneously in the trap.

The energy of each RR x ray is equal to the sum of the incident electron energy and the ionization potential of the recombined ion. The RR x-ray lines from capture into the K shell of bare and hydrogenlike high-Z ions can be resolved in a germanium detector, allowing a measurement of the ground-state ionization potential difference between the hydrogenlike and heliumlike ions. If a high-Z and a low-Z element are present in the trap simultaneously, then the ionization potential difference between the high-Z and low-Z ions can be obtained. An absolute measurement of a single ionization potential is not possible at an interesting level of precision because the uncertainty in the electron beam energy is too great.

A. Apparatus

The Super EBIT is described in detail elsewhere [15]. Briefly, ions are confined radially by the negative space-charge potential of an electron beam. Axial confinement is achieved by voltages applied to three drift tubes (i.e., trap electrodes); typically the end electrodes are on the order of 100 V more positive than the center electrode and the ions are confined to a length of roughly 2 cm along the beam. The electron beam is compressed to a diameter of 70 μm by a 3-T magnetic field. The trapped ions, injected in low charge states or as neutral vapors, are ionized to high charge states by successive collisions with beam electrons. X rays from electron-ion collisions are observed through a slot in the center trap electrode and through a beryllium vacuum window.

Three different hyperpure-germanium x-ray detectors were used in the present experiments. One was a 1.0-cm-thick planar detector and the other two were coaxial detectors with thicknesses of 1.9 and 3.1 cm. The detectors were located in a lead shield as shown in Fig. 1. Although the RR lines of interest are in a clean spectral region above the end point of bremsstrahlung from the electron beam, the lead shield restricts the field of view of the detector to the ion trapping region and protects the detector from a high rate of bremsstrahlung occasionally produced elsewhere in the apparatus. To ensure an accurate energy calibration, radiaoactive calibration sources were located as shown in Fig. 1 and counted simultaneously with the trapped-ion x rays. Doppler shifts are completely absent for trapped EBIT ions and Doppler broadening is negligible.

Six different elements were studied at several different electron beam energies as summarized in Table I. Germanium, dysprosium, and bismuth were injected into the trap as low-charge ions from a vacuum-spark ion source [16]. There was a delay of several seconds between ion injection and the start of data acquisition to allow for stripping to the bare and hydrogenlike charge states. Data acquisition times were either 14 or 35 s, depending on conditions, after which the trap was dumped and the cycle repeated.

Xenon was injected as a collimated beam of neutral gas atoms directed at a 90° angle to the electron beam. Roughly 0.2% of the xenon atoms that intercept the electron beam are ionized and captured. Even though the injection (and loss) of xenon is a steady-state process, the trap was dumped periodically to avoid the accumulation of contaminant elements.

Two of the elements studied (tungsten and osmium) and a third that was not studied (barium) are available fortuitously without injection. They originate from the cathode of the electron gun, probably by ion sputtering, and slowly accumulate in the trap with a filling time on the order of 100 s or more. Tungsten and osmium were studied by turning off the periodic dumping of the trap and running in a steady-state mode.

B. X-ray measurements

An x-ray spectrum for tungsten and osmium is shown in Fig. 2. This spectrum is the sum of several individual runs

TABLE I. Energies (in keV), calibration sources, and detectors used for the measurements of RR energies.

Element (Z)	H-like ionization potential	Beam energy	Bare→H-like RR energy	Calibration lines (source)	Detector type (thickness)
Ge (32)	14.1	31.4	45.5	22.1 (Ag $K\alpha$), 59.5 (^{241}Am)	planar (1.0 cm)
		38.6	52.7	22.1 (Ag $K\alpha$), 59.5 (^{241}Am)	planar (1.0 cm)
Xe (54)	41.3	85.6	126.9	110 (^{169}Yb), 130 (^{169}Yb)	planar (1.0 cm)
		139.8	181.1	177 (^{169}Yb), 198 (^{169}Yb)	coaxial (1.9 cm)
		140.8	182.1	177 (^{169}Yb), 198 (^{169}Yb)	coaxial (3.1 cm)
		141.0	182.3	177 (^{169}Yb), 198 (^{169}Yb)	planar (1.0 cm)
		141.8	183.1	179 (^{182}Ta), 198 (^{182}Ta)	coaxial (1.9 cm)
		168.3	209.6	198 (^{169}Yb), 308 (^{169}Yb)	coaxial (3.1 cm)
		182.6	223.9	198 (^{169}Yb), 308 (^{169}Yb)	coaxial (1.9 cm)
		183.6	224.9	198 (^{169}Yb), 308 (^{169}Yb)	coaxial (1.9 cm)
Dy (66)	63.1	168.4	231.5	198 (^{169}Yb), 308 (^{169}Yb)	coaxial (1.9 cm)
W (74)	80.8	184.9	265.7	177 (^{169}Yb), 308 (^{169}Yb)	coaxial (1.9 cm)
Os (76)	85.6	184.9	270.5	177 (^{169}Yb), 308 (^{169}Yb)	coaxial (1.9 cm)
Bi (83)	104.1	182.6	286.7	198 (^{169}Yb), 308 (^{169}Yb)	coaxial (1.9 cm)
		183.6	287.7	198 (^{169}Yb), 308 (^{169}Yb)	coaxial (1.9 cm)
		191.6	295.7	198 (^{169}Yb), 308 (^{169}Yb)	coaxial (1.9 cm)

obtained during a total counting time of 16 h with beam currents of 195–210 mA at 185 keV, which is representative of the conditions used for the other elements. The spectrum shows RR lines from tungsten, osmium, and barium, as well as lines from the ^{169}Yb radioactive source used for calibration. At an x-ray energy equal to the electron-beam energy, RR into high Rydberg levels joins smoothly with bremsstrahlung from the target ions, which dominates the spectrum at lower energies. Although K-shell x rays appear in our spectra, they are not useful for energy measurements because they contain unresolved contributions from several charge states.

The 900 eV full width at half maximum (FWHM) of the tungsten and osmium RR ($n=1$) lines is dominated by the resolution of the 1.9-cm-thick coaxial detector used to obtain the spectrum of Fig. 2; the energy spread of the electron beam is roughly 100 eV. X-ray spectra were saved at intervals of 2 h or less and examined for drifts in beam energy or in the electronic gain. Observed drifts were on the order of 200 eV or less in a 24-h period, so spectra were summed in groups of similar runs and analyzed. The observed RR line energies are insensitive to electronic gain drift because the calibration lines are accumulated simultaneously. Our measured difference in RR line energies is also insensitive to any drift in the incident electron energy because an energy drift affects all RR lines equally.

Several calibration sources were used to span the range of x-ray energy used in the present work. They are listed in

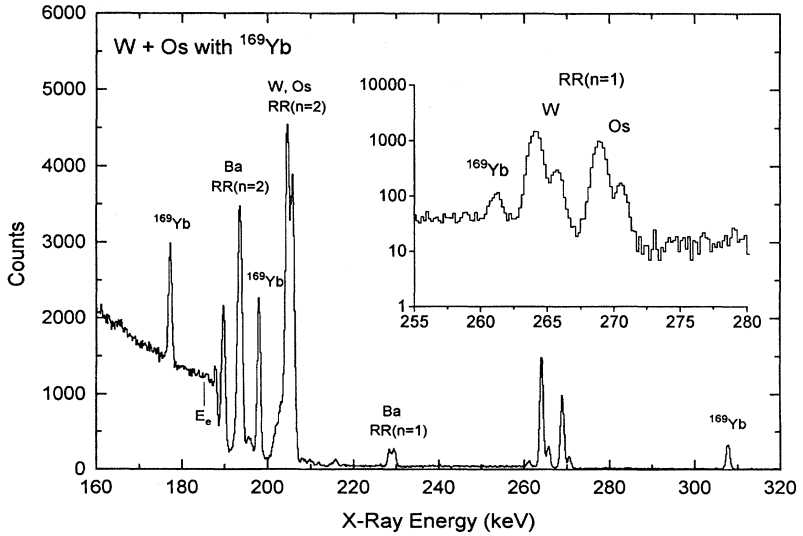

FIG. 2. X-ray spectrum used to determine the hydrogenlike and heliumlike ionization potential differences for tungsten and osmium. The ^{169}Yb lines are from the calibration source; all other x rays come from electron-ion collisions in the trap at an electron energy of $E_e=185$ keV. The expanded inset shows the tungsten and osmium RR ($n=1$) features on a logarithmic scale. The doublet for each element corresponds to capture on both bare and hydrogenlike target ions.

TABLE II. Calibration energies (in eV) used in the present work.

Source	Line energy
Ag $K\alpha_{1,2}$	22 105.3 [a]
^{241}Am	59 537 [b]
^{169}Yb	109 779.87±0.29 [c]
	130 523.68±0.34 [c]
	177 214.02±0.46 [c]
	197 957.88±0.52 [c]
	307 737.57±0.80 [c]
^{182}Ta	100 106.5±0.3 [d]
	152 430.8±0.5 [d]
	156 387.4±0.5 [d]
	179 394.8±0.5 [d]
	198 353.0±0.6 [d]
	222 109.9±0.6 [d]
	229 322.0±0.9 [d]
	264 075.5±0.8 [d]

[a]Weighted average of $K\alpha_1$ and $K\alpha_2$; Ref. [27].
[b]Reference [27].
[c]Reference [28].
[d]Reference [29].

Table II along with adopted values for the calibration energies. The ^{169}Yb (32-day half-life) and ^{182}Ta (115-day half-life) sources were made by placing pieces of ytterbium and tantalum metal next to a ^{252}Cf neutron source for several weeks. These sources were used in the geometry of Fig. 1 and their activity level was chosen so that the count rate in the source lines was of the same order as that in the RR lines of interest. The ^{241}Am and Ag K-shell x-ray-fluorescence sources, used only for the germanium RR ($n=1$) splitting, were commercial sources. They were counted in separate runs interleaved with the RR x-ray runs. Relatively short counting periods minimized any gain drift.

Line centroid positions were determined from least-squares fits using a peak shape consisting of a Gaussian plus a shelf on the low-energy side of the peak. This fitting function has been found previously to be a good representation of the peak shape from solid-state x-ray detectors [17]. A linear background was subtracted. None of our fits showed a statistically significant deviation from this shape, including several fits to intense lines from radioactive sources. The widths of the barely resolved RR ($n=1$) lines from bare and hydrogenlike target ions were constrained to be the same in the fitting procedure. Calibration lines from the radioactive sources were fitted separately with an independent width.

Sample RR ($n=1$) lines from typical data runs for germanium, dysprosium, and bismuth are shown in Fig. 3. The large change in the relative intensity of the peak from bare target ions between germanium and bismuth is due to the rapidly decreasing $1s$ ionization cross sections for very heavy elements. At present, this prevents us from extending these measurements to elements beyond $Z=83$. Spectra from individual data runs were summed together in similar groups, examined for consistency, and analyzed as above. To check for the possible presence of an undetected background feature that could shift one of the peak centroids, germanium data were obtained at two different electron-beam energies (i.e., different RR energies) and bismuth data were obtained at three different energies as listed in Table I. In addition, background runs were taken with the injection of these elements turned off in order to ensure that no other lines interfered with the RR transitions.

Xenon data were obtained at a large number of different conditions as listed in Table I. These included the use of three different detectors, several different electron energies, and four different pairs of calibration lines. Sample spectra at three different energies are shown in Fig. 4, where it is possible to see the different position of the xenon RR lines with respect to the calibration lines and the changing relative intensity of the RR ($n=1$) lines from bare and hydrogenlike target ions. All of the different conditions gave consistent values for the RR ($n=1$) line splitting, so the individual runs were combined to obtain a final xenon value.

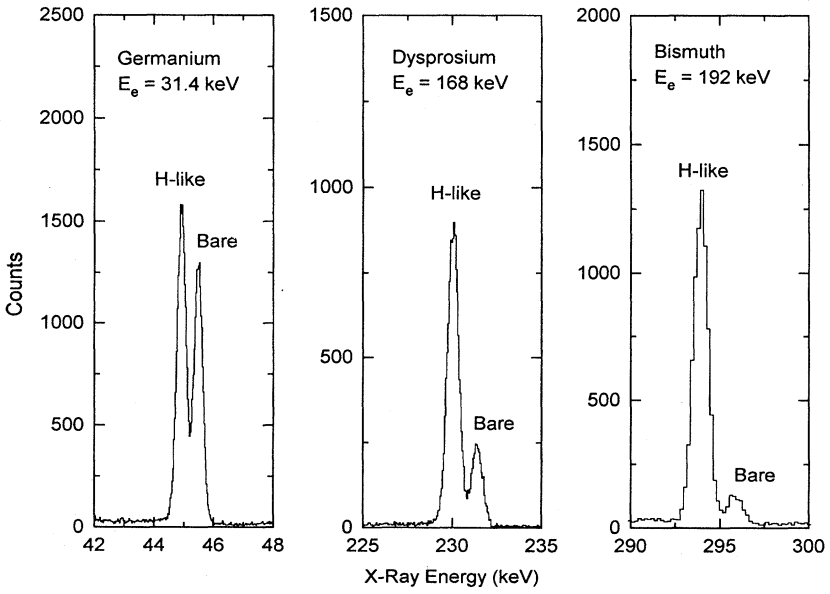

FIG. 3. K-shell RR lines for germanium, dysprosium, and bismuth as observed in typical runs.

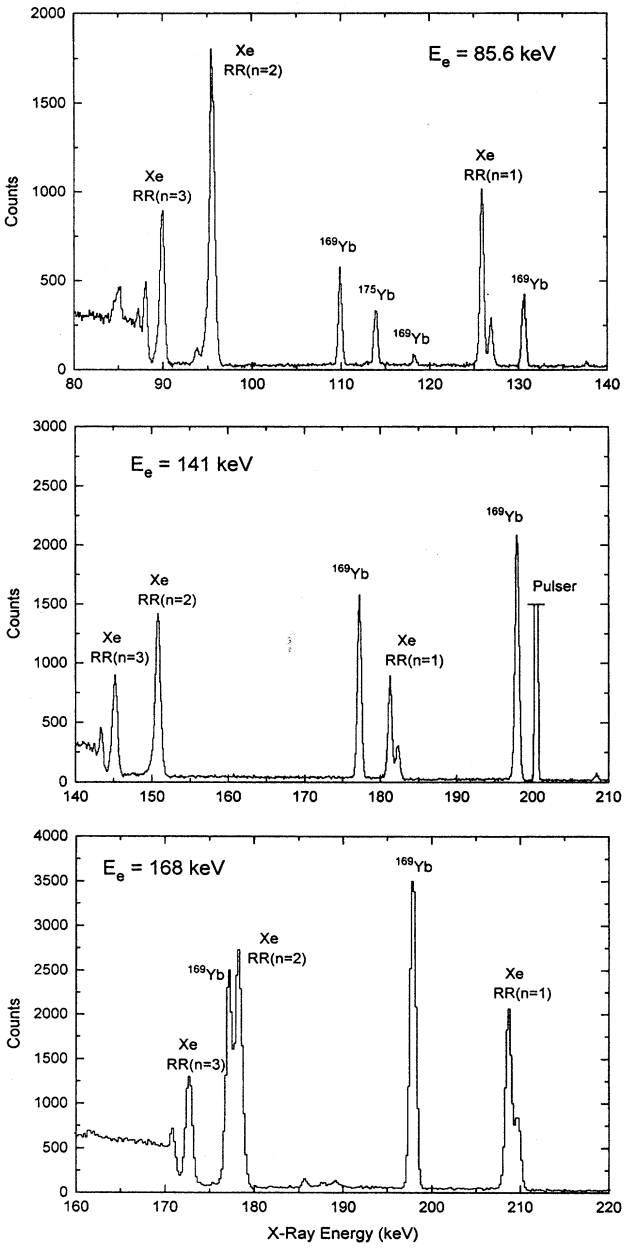

FIG. 4. Three examples of the different combinations of electron energy and detector used for the xenon measurements. Top and middle: 1-cm-thick planar detector. Bottom: 3-cm-thick coaxial detector. Electron energies are as labeled.

Since most of the elements studied have isotopes with nonzero nuclear spin, there is a hyperfine splitting of the ground-state energy in the hydrogenlike ion. RR of bare target ions populates the two hydrogenlike hyperfine states statistically, so there is no hyperfine shift of the "bare RR" peak centroid. However, hydrogenlike target ions are always in the lower hyperfine level, so there is a hyperfine shift of the "hydrogenlike RR" peak to lower x-ray energy, corresponding to the energy radiated away in previous decays of the upper hyperfine level in the target ions. This shift is less than 0.1 eV and has been neglected for all of the elements studied except for bismuth. For bismuth we used the recently measured hyperfine splitting [18] to deduce an upward correction of 2.79 eV, which we applied to the position of the hydrogenlike RR line. (Based on the 0.35-ms hyperfine lifetime of hydrogenlike ^{209}Bi [18] and an estimated rate of approximately 1 Hz for populating the upper hyperfine level in our Super EBIT, the probability of finding a hydrogenlike bismuth target ion in the upper hyperfine level is less than or equal to 10^{-3}.)

C. Bismuth-xenon separation

We have also obtained data for the ionization potential difference between heliumlike bismuth ($Z=83$) and xenon ($Z=54$). Since most contributions to the energy are much larger at $Z=83$ than at $Z=54$, this measurement mainly provides information about bismuth.

Hydrogenlike bismuth and xenon target ions were trapped simultaneously by leaving the xenon gas injection on continuously during the normal bismuth run cycle described above. Two different electron-beam energies (142 and 184 keV) and two different calibration sources (^{169}Yb and ^{182}Ta) were used in order to place the RR lines in different locations with respect to the calibration lines as a consistency check. Sample spectra from the different conditions are shown in Fig. 5. Since only the heliumlike-bismuth ionization potential is of interest in these data, the results of our separate heliumlike-hydrogenlike splitting measurements were used to constrain the separation of the two RR ($n=1$) components during the bismuth-xenon difference fits. A hyperfine correction of $+2.79$ eV was applied to the bismuth line energy as described above.

III. SOURCES OF ERROR

The results reported in Table III required a determination of the centroids of x-ray lines to an accuracy on the order of 1% of the FWHM of the peak and 2×10^{-5} of the total x-ray energy. Several sources of systematic error were considered and dealt with using consistency checks and data collection procedures as described below. In the end, the overall uncertainties in our results are dominated by the statistical uncertainty in the line centroid positions and the contribution of systematic errors is minor. Runs at different beam energies and with different detectors, as described above, were performed to reveal unrecognized sources of error such as structure in the spectral background. Here we describe our investigation of several known sources of error.

The possible sources of error in the present work can be divided into two general categories: effects common to any x-ray and γ-ray energy measurement with solid-state detectors and effects specific to the EBIT environment. The present technique is closely related to the "mixed source" technique used to measure absolute γ-ray energies to 1-eV accuracy in the same energy range [19]. Many sources of error have been addressed more carefully in that context. Effects unique to the EBIT environment consist of space-charge shifts in the electron energy, possible spectator electrons on the target ions, and time-dependent spectral changes.

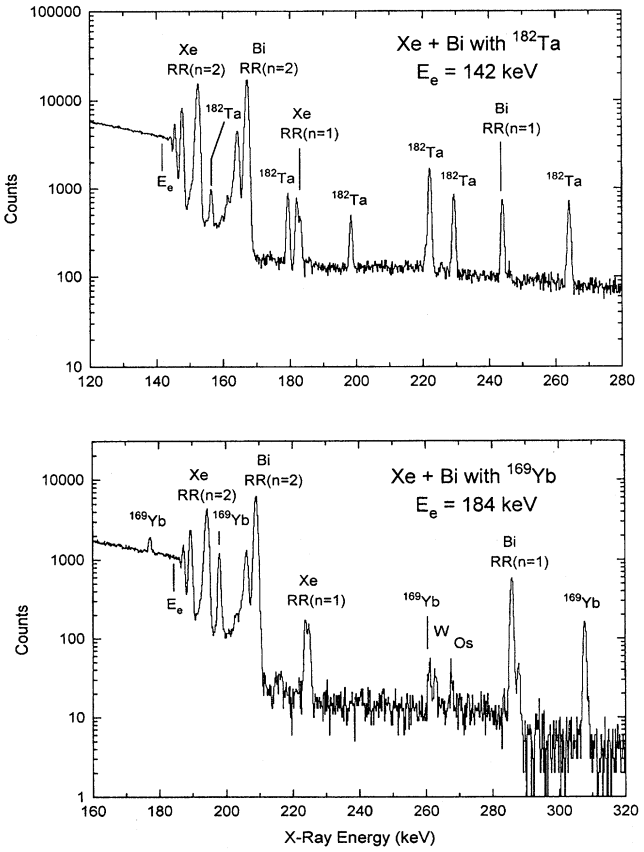

FIG. 5. Sample spectra used to determine the difference in the ionization potentials of heliumlike bismuth and xenon. Top: $E_e = 142$ keV with a ^{182}Ta calibration source. Bottom: $E_e = 184$ keV with a ^{169}Yb calibration source. Both spectra were obtained with the 2-cm-thick coaxial detector.

A. Energy calibration

The energies of the ^{169}Yb and ^{182}Ta calibration lines are known to 0.8 eV or better (see Table II), but a nonlinearity in the electronics or detector response could result in a much larger energy error at energies away from the calibration lines. For each data set, the two closest clean calibration lines, as listed in Table I, were used to determine a linear energy scale for the RR lines. Because the two components of the RR ($n=1$) spectral feature are closely spaced, nonlinearity is not important for the determination of the RR ($n=1$) splitting. However, it is important for determining the 62-keV bismuth-xenon-ray energy difference. In this case a curvature or quadratic correction to the energy scale was determined from long high-statistics runs with the radioactive sources and applied to the bismuth-xenon data. This correction amounted to about 4 eV for the ^{182}Ta-calibrated data and less than 1 eV for the ^{169}Yb-calibrated data, where the relative positions of the RR and calibration lines reduced the effect. The uncertainty in this correction has been neglected.

B. Peak shape and fitting function

As mentioned above, the fitting function consists of a Gaussian peak shape with a shelf on the low-energy side. The bare and hydrogenlike RR ($n=1$) peaks partially overlap and their apparent centroid separation could be affected by a deviation of the actual peak shape from the fitting function due to "pileup tails." This was monitored by including a pulser peak in the spectra at a count rate more than ten times faster than the RR lines. No tails were observed on the pulser peak, implying that there were none on the RR ($n=1$) peaks. Aluminum absorber sheets with a total thickness varying from 0.25 to 1.75 mm were used to attenuate low-energy x rays and maintain a total full-spectrum count rate on the order of 200 counts/s.

Although the fitting function was tested with fits to high-statistics source lines, the approximately 100-eV energy spread of the electron beam only affects the RR lines. We assumed that the beam energy spread, as well as any small peak-broadening contributions from noise or gain drift, could be accounted for by allowing the Gaussian width of the x-ray peak to be a free parameter during the fitting procedure. This choice is supported by the fact that residuals from all of the RR fits showed no deviation from the chosen peak shape, including data sets with very different ratios of the bare and hydrogenlike components of the RR ($n=1$) feature.

TABLE III. Two-electron contributions to the ground-state energy of heliumlike ions (in eV). The last row is the difference in the ionization potentials of heliumlike bismuth and xenon.

		Theory				
Element (Z)	Experiment	Relativistic [a] MBPT	Relativistic [b] all order	MCDF [c]	Unified [d]	Expt.−Theor. [c]
Ge (32)	562.5±1.6	561.9	562.1	562.1	562.1	0.4±1.6
Xe (54)	1 027.2±3.5	1028.1	1028.4	1 028.2	1 028.8	−1.0±3.5
Dy (66)	1 341.6±4.3	1336.6	1337.2	1 336.5	1 338.2	5.1±4.3
W (74)	1 568±15	1574.6	1574.8	1 573.6	1 576.6	−6±15
Os (76)	1 608±20		1639.2	1 637.8	1 641.2	−30±20
Bi (83)	1 876±14	1882.7		1 880.8	1 886.3	−5±14
Bi-Xe	61 984.0±8.2			61 980.5	61 975.6	3.5±8.2

[a]Reference [6].
[b]Reference [9], using hydrogenlike energies from Ref. [5].
[c]References [30,7].
[d]Reference [22], using hydrogenlike energies from Ref. [5].

C. Electronic stability

Large changes in the RR ($n=1$) count rate during the data acquisition period (compared to the constant rate in the calibration lines) could lead to a systematic error if there were a time-dependent gain shift. This was checked by dividing the data acquisition into seven separate time bins and comparing centroid positions in the first time bin with the average of the other six. No statistically significant differences were found. The first time bin was selected because that is where the RR ($n=1$) rate is most different (lower) due to the still-evolving ionization balance. A successive-approximation analog-to-digital converter (ADC) was used to achieve the time routing. A second (Wilkinson-type) ADC was used simultaneously for roughly half the data runs, but it could not be time routed. A cross-check demonstrated consistency between results from the two ADC's.

D. Detector geometry

Previous studies have shown that the centroid positions of γ-ray peaks in germanium detectors can depend on the incident photon direction [20]. Our detector directly faced the trapped ions, but the calibration sources were placed in an annulus that subtended a half angle of approximately 3.5° with respect to the detector axis. Although we do not expect a significant centroid shift at our x-ray energies with this geometry, we performed a test with a comparison source moved between angles of 0° and 40°. No shift was found to a precision of 4 eV, suggesting that any shift at 3.5° is negligible. Note that this type of error could affect the bismuth-xenon energy difference, but would not contribute to the measured splitting of the closely spaced RR ($n=1$) lines.

E. Space-charge potential

The bismuth-xenon energy-difference measurement raises an additional concern that is not present for the RR ($n=1$) splitting measurements. If the bismuth and xenon ions were located at different beam radii, they would experience slightly different electron-beam energies due to the space-charge potential of the beam. As a result, the measured difference between their RR x rays would be shifted. The space-charge voltage difference between the center and edge of the electron beam is typically 7 V for the conditions used. The difference in the average electron energy experienced by the bismuth and xenon ions is much less than this because both kinds of ions are smoothly distributed across the beam profile. A similar argument applies to the change in electron energy at the axial trap barriers. Uncertainty in the ion temperatures prevents an exact calculation of this effect, but the overall contribution to the bismuth-xenon energy difference is estimated at no more than 1 eV and has been neglected. A related error could occur if there were a change in the total space-charge potential during the data acquisition period due to a change in the number of trapped ions, thus causing a change in the incident electron energy. (The total electron space-charge potential at the axis of the trap is typically 75 V.) If the relative RR ($n=1$) count rates from bismuth and xenon changed as well, then the different weightings could produce a change in the apparent bismuth-xenon energy difference. This effect was avoided by operating the trap in a manner that minimized count rate changes. Centroid separations were compared for early and late time bins and no differences were found.

F. Spectator electrons

The ionization potentials are deduced from radiative recombination peak energies assuming that electrons are captured onto the ground states of bare and hydrogenlike ions. The centroid energy of these peaks could be shifted by the presence of additional electrons in high Rydberg levels, an effect observed for $K\alpha$ transitions in hot plasmas [21]. It is easy to show that this effect is insignificant for bare and hydrogenlike EBIT ions. The population rate of Rydberg states by RR, charge exchange with neutral atoms, and electron impact excitation is on the order of 1 Hz per ion based on estimated RR and excitation cross sections and a charge-exchange recombination rate estimated from its effect on the ionization balance. The resonant process of dielectronic recombination does not occur at our electron energies. The time scale for the cascade decay of a high-n state ($n\sim400$) is of the order of 10–100 ns; thus the probability of RR ($n=1$) on an ion with an electron in such a high Rydberg state is less than 10^{-7}.

We conclude that the systematic uncertainty from all sources of error is small compared to the statistical uncertainty of the peak centroid determination. Therefore our quoted uncertainties are entirely statistical.

IV. RESULTS AND DISCUSSION

All of the individual data sets for each element have been combined to obtain a final value for the difference in ionization potential between the heliumlike and hydrogenlike ionization stages. The results are presented in Table III, where they are compared with theoretical calculations. The measured difference between the heliumlike ionization potential of bismuth and xenon is also listed in Table III.

A. Theoretical predictions

Several different theoretical approaches have been applied to heliumlike ions. The "unified" method of Drake uses a relativistic $1/Z$ expansion [22]. This approach is known to be incomplete at the level of $(Z\alpha)^4$, so it is expected to be most accurate at low Z with an uncertainty that grows like Z^4. The multiconfiguration Dirac-Fock (MCDF) [7,23] and relativistic many-body perturbation theory (MBPT) [6,24] approaches are more appropriate for high-Z systems. Recently an all-order technique for relativistic MBPT has been applied to heliumlike ions [9]. Results from these four theoretical approaches are compared to our measured two-electron contributions to the heliumlike ground-state energies in Table III. The results from the all-order and unified theories are available as total ionization energies for the heliumlike ground state, so it is necessary to subtract the (more accurate) hydrogenlike energy to obtain the two-electron contribution. We used the hydrogenlike energies of Johnson and Soff for this purpose [5].

As can be seen in Table III, there is a general agreement between our experimental results and the predictions of all four theories. The experimental uncertainties prevent a clear distinction among the different theories. However, at higher Z, our results favor the MBPT, all-order, and MCDF theories

TABLE IV. Comparison between the relativistic MBPT calculations of Lindgren *et al.* [6] and the present measurements (in eV).

Element (Z)	Second-order many body	Two-electron Lamb shift	Total theory	Experiment
Ge (32)	−5.2	−0.5	561.9	562.5±1.6
Xe (54)	−6.9	−1.6	1028.1	1027.2±3.5
Dy (66)	−8.6	−2.5	1336.6	1341.6±4.3
W (74)	−9.4	−3.4	1574.6	1568±15
Bi (83)	−11.0	−4.5	1882.7	1876±14

over the unified theory. A recently developed relativistic configuration-interaction theory has been very successful in calculating $n=2$ to $n=2$ transitions in heliumlike ions [8]. This theory is not included in Table III because results are not available for most of the ions we studied; however, it is in agreement with the other theories. We note that, although our result for the bismuth-xenon ionization potential difference is not a direct measurement of the two-electron contributions, its uncertainty is smaller than that of the bismuth-only result.

The individual two-electron contributions to the ground-state energy of heliumlike ions in relativistic MBPT have recently been calculated by Lindgren *et al.* [6]; we list them in Table IV along with our experimental results. Our experimental uncertainties are smaller than the second-order many-body contribution (except at higher Z), so our results mostly test this part of the theory. Our uncertainties are only slightly larger than the two-electron (screened) Lamb shift, particularly for dysprosium and xenon.

B. Other experiments

Until now, the only available technique for the study of the ground-state energies of heliumlike ions has been the spectroscopy of $K\alpha$ transitions. Due to the strong $1/n^3$ scaling of the leading QED effects [see Eq. (1)], this method tests the total ground-state QED contributions by assuming that the energies of the excited levels can be calculated precisely. For heliumlike Ge^{30+} a Bragg crystal spectrometer was used in a previous EBIT measurement to obtain an accuracy of 0.2 eV for the $1s2p(^1P_1)$-$1s^2(^1S_0)$ transition, enabling a distinction between different theories [25]. This transition has also been measured in heliumlike Kr^{34+} with an accuracy of 0.3 eV [26].

At higher Z, all available heliumlike transition energy measurements have been done using high-velocity accelerator beams capturing electrons from neutral target atoms. These experiments must deal with large Doppler shifts and the fact that the observed $K\alpha_1$ and $K\alpha_2$ lines both contain two transitions that are unresolved in existing experiments. In spite of these problems, uncertainties as low as 60 eV have been obtained for heliumlike bismuth [11] and uranium [12] and 3.5 eV for xenon [10].

It should be noted that heliumlike $K\alpha$ energies are dominated by the one-electron (hydrogenlike) energy. In contrast, the energy differences measured in the present work isolate the true two-electron contributions. This will become even more important as the experimental precision improves and smaller contributions can be tested.

V. SUMMARY

We have used a recently developed experimental approach to obtain the first direct measurements of the two-electron contributions to the ground-state energy of high-Z heliumlike ions. Our results support theoretical calculations within the experimental uncertainties. The technique used in the present work is limited by the x-ray intensity and charge states available from the Super EBIT device and it is possible that the uncertainties for the heaviest elements could be reduced by an order of magnitude if more x-ray intensity were available. In this case, the smaller and uncalculated two-electron contributions to heliumlike energies could be measured.

ACKNOWLEDGMENTS

We thank D. Knapp for expert assistance with a computer interface used to obtain part of the data. We also thank P. Indelicato and I. Lindgren for providing calculated energies and allowing us to use them prior to publication. We gratefully acknowledge helpful discussions with M. H. Chen. This work was performed under the auspices of the U.S. Department of Energy by Lawrence Livermore National Laboratory under Contract No. W-7405-Eng-48.

[1] P. J. Mohr, Phys. Rev. A **46**, 4421 (1992); Nucl. Instrum. Methods B **9**, 459 (1985).

[2] H. F. Beyer, D. Liesen, F. Bosch, K. D. Finlayson, M. Jung, O. Klepper, R. Moshammer, K. Beckert, H. Eickhoff, B. Franzke, F. Nolden, P. Spädtke, M. Steck, G. Menzel, and R. D. Deslattes, Phys. Lett. A **184**, 435 (1994).

[3] H. F. Beyer, IEEE Trans. Instrum. Meas. **44**, 510 (1995).

[4] Th. Stöhlker, P. H. Mokler, K. Beckert, F. Bosch, H. Eickhoff, B. Franzke, M. Jung, T. Kandler, O. Klepper, C. Kozhuharov, R. Moshammer, F. Nolden, H. Reich, P. Rymuza, P. Spädtke, and M. Steck, Phys. Rev. Lett. **71**, 2184 (1993).

[5] W. R. Johnson and G. Soff, At. Data Nucl. Data Tables **33**, 405 (1985).

[6] I. Lindgren, H. Persson, S. Salomonson, and P. Sunnergren,

Proceedings of the Nobel Symposium on Trapped Charged Particles and Related Fundamental Physics, Lysekil, 1994 [Phys. Scr. (to be published)].

[7] O. Gorceix, P. Indelicato, and J. P. Desclaux, J. Phys. B **20**, 639 (1987); P. Indelicato, O. Gorceix, and J. P. Desclaux, *ibid.* **20**, 651 (1987).

[8] K. T. Cheng, M. H. Chen, W. R. Johnson, and J. Sapirstein, Phys. Rev. A **50**, 247 (1994); M. H. Chen, K. T. Cheng, and W. R. Johnson, *ibid.* **47**, 3692 (1993).

[9] D. R. Plante, W. R. Johnson, and J. Sapirstein, Phys. Rev. A **49**, 3519 (1994).

[10] J. P. Briand, P. Indelicato, A. Simionovici, V. San Vicente, D. Liesen, and D. Dietrich, Europhys. Lett. **9**, 225 (1989).

[11] Th. Stöhlker, P. H. Mokler, H. Geissel, R. Moshammer, P. Rymuza, E. M. Bernstein, C. L. Cocke, C. Kozhuharov, G. Münzenberg, F. Nickel, C. Scheidenberger, Z. Stachura, J. Ullrich, and A. Warczak, Phys. Lett. A **168**, 285 (1992).

[12] P. H. Mokler, Th. Stöhlker, C. Kozhuharov, R. Moshammer, P. Rymuza, F. Bosch, and T. Kandler, Phys. Scr. **T51**, 28 (1994).

[13] J. P. Briand, P. Chevallier, P. Indelicato, K. P. Ziock, and D. D. Dietrich, Phys. Rev. Lett. **65**, 2761 (1990).

[14] R. E. Marrs, S. R. Elliott, and D. A. Knapp, Phys. Rev. Lett. **72**, 4082 (1994).

[15] D. A. Knapp, R. E. Marrs, S. R. Elliott, E. W. Magee, and R. Zasadzinski, Nucl. Instrum. Methods Phys. Res. Sect. A **334**, 305 (1993).

[16] I. G. Brown, J. E. Galvin, R. A. MacGill, and R. T. Wright, Appl. Phys. Lett. **49**, 1019 (1986).

[17] L. C. Longoria, A. H. Naboulsi, P. W. Gray, and T. D. MacMahon, Nucl. Instrum. Methods Phys. Res. Sect. A **299**, 308 (1990).

[18] I. Klaft, S. Borneis, T. Engel, B. Fricke, R. Grieser, G. Huber, T. Kühl, D. Marx, R. Neumann, S. Schröder, P. Seelig, and L. Völker, Phys. Rev. Lett. **73**, 2425 (1994).

[19] R. G. Helmer, A. J. Caffrey, R. J. Gehrke, and R. C. Greenwood, Nucl. Instrum. Methods **188**, 671 (1981).

[20] R. G. Helmer, R. J. Gehrke, and R. C. Greenwood, Nucl. Instrum. Methods **123**, 51 (1975).

[21] M. Bitter, H. Hsuan, V. Decaux, B. Grek, K. W. Hill, R. Hulse, L. A. Kruegel, D. Johnson, S. von Goeler, and M. Zarnstorff, Phys. Rev. A **44**, 1796 (1991).

[22] G. W. Drake, Can. J. Phys. **66**, 586 (1988).

[23] I. P. Grant, B. J. McKenzie, P. H. Norrington, D. F. Mayers, and N. C. Pyper, Comput. Phys. Commun. **21**, 207 (1980); B. J. McKenzie, I. P. Grant, and P. H. Norrington, *ibid.* **21**, 233 (1980).

[24] W. R. Johnson and J. Sapirstein, Phys. Rev. A **46**, R2197 (1992).

[25] S. MacLaren, P. Beiersdorfer, D. A. Vogel, D. Knapp, R. E. Marrs, K. Wong, and R. Zasadzinski, Phys. Rev. A **45**, 329 (1992).

[26] P. Indelicato, J. P. Briand, M. Tavernier, and D. Liesen, Z. Phys. D **2**, 249 (1986).

[27] *Table of Isotopes*, 7th ed., edited by C. M. Lederer and V. S. Shirley (Wiley, New York, 1978).

[28] E. G. Kessler, L. Jacobs, W. Schwitz, and R. D. Deslattes, Nucl. Instrum. Methods **160**, 435 (1979).

[29] R. G. Helmer, P. H. M. Van Assche, and C. Van Der Leun, At. Data Nucl. Data Tables **24**, 39 (1979).

[30] P. Indelicato (private communication).